Reconnection properties in collisionless plasma with open boundary conditions

H. E. Sun, Z. W. Ma, and J. Huang

Citation: Physics of Plasmas **21**, 072115 (2014); doi: 10.1063/1.4889894
View online: http://dx.doi.org/10.1063/1.4889894
View Table of Contents: http://scitation.aip.org/content/aip/journal/pop/21/7?ver=pdfcov
Published by the AIP Publishing

Reconnection properties in collisionless plasma with open boundary conditions

H. E. Sun (孙宏恩),[1] Z. W. Ma (马志为),[1,2,a)] and J. Huang (黄俊)[2]
[1]*Institute of Plasma Physics, Chinese Academy of Sciences, Hefei 230031, China*
[2]*Institute for Fusion Theory and Simulation, Zhejiang University, Hangzhou 310027, China*

(Received 10 April 2014; accepted 30 June 2014; published online 15 July 2014)

Collisionless magnetic reconnection in a Harris current sheet with different initial thicknesses is investigated using a $2\frac{1}{2}$-D Darwin particle-in-cell simulation with the magnetosonic open boundary condition. It is found that the thicknesses of the ion dissipation region and the reconnection current sheet, when the reconnection rate E_r reaches its first peak, are independent of the initial thickness of the current sheet; while the peak reconnection rate depends on it. The peak reconnection rate increases with decrease of the current sheet thickness as $E_r \sim a^{-1/2}$, where a is the initial current sheet half-thickness. © *2014 AIP Publishing LLC*. [http://dx.doi.org/10.1063/1.4889894]

I. INTRODUCTION

Magnetic reconnection is a basic plasma process which leads to the rapid conversion of magnetic field energy into kinetic and thermal energy, accompanying with the change of the topology of the magnetic field.[1] Magnetic reconnection is widely believed to play a crucial role in dynamic processes occurred in the magnetospheres, the solar corona, and laboratory experiments. Through several decade studies of magnetic reconnection, we have greatly advanced our understanding of magnetic reconnection process, but there are many fundamental questions regarding to collisionless reconnection still remaining to be understood. Since there is no first-principle theory to address the fundamental questions, simulations and scaling arguments are used to understand magnetic reconnection.[2–9]

Up to now, the model that places considerable emphasis on the effect of the Hall physics to explain fast reconnection is widely accepted. Especially, an important conclusion of Geospace Environment Modelling (GEM) challenge,[9–16] by comparing a series of the simulation results obtained using resistive MHD, Hall MHD, hybrid, and particle-in-cell (PIC) codes, is that the reconnection rate, much larger than the resistive MHD reconnection rate with a uniform resistivity, is primarily determined by the Hall term and insensitive to the dissipation mechanisms. Ugai and Tsuda[17] demonstrated that fast MHD reconnection is realized if anomalous resistivity is localized around X neutral point. In recent years, there was ongoing debate whether the reconnection rate depends on the system size.[6,18–20] Some researchers have argued that the Hall mediated reconnection rate is independent of the system size;[6,8,18] while others have found a significant dependence by scaling analysis and Hall MHD simulation.[19,20] But there is still no compelling simulation scaling result with PIC simulation.

In previous fully kinetic PIC simulations, period boundary conditions are usually imposed at the plasma outflow boundaries. Because of the collision of the opposite jet flows and the accumulation of the reconnected magnetic flux in the O-point region, the periodic boundary condition is only meaningful for the early period of the reconnection process.[21,22] To make progress, many researchers focus on developing new open boundary model, which is a difficult problem. Daughton *et al.*[21] developed a new model with an electromagnetic boundary condition to permit electromagnetic radiation to leave the system and showed that at early stage the results are in excellent agreement with previous work with periodic boundaries, while the evolution over a longer time is quite different. Huang and Ma[23] noted that the electromagnetic wave is ignored in the Darwin model, which is always used in the low frequency PIC simulation, and argued that the local Alfvén velocity, instead of the light speed, should be more appropriate to be used to fix the inflow boundary condition, since Alfvén wave is the dominant wave in a magnetized plasma.

In this paper, a $2\frac{1}{2}$-D Darwin PIC code, which is an open boundary model with the Alfvén velocity condition in the inflow boundary, is used to study the scaling law between the initial current sheet width and the peak reconnection rate. The paper is organized as follows. The Darwin PIC simulation model with open boundary conditions with both the inflow and outflow boundaries is introduced in Sec. II. In Sec. III, we compare the magnetic reconnection process in systems with different initial current sheet thickness, and also the effects of different inflow boundary conditions are presented. Finally, the conclusion is given in Sec. IV.

II. SIMULATION MODEL

The simulation model is based on a $2\frac{1}{2}$-D Darwin PIC simulation model, with the two dimensions in the configuration space (x and z) and the three dimensions in the canonical momentum space (p_x, p_y, and p_z), which has been employed in the earlier studies.[24–28] The particle motion equations are as follows:

$$\frac{d\mathbf{P}_\alpha}{dt} = \frac{q_\alpha}{m_\alpha}(\nabla\mathbf{A})\cdot(\mathbf{P}_\alpha - q_\alpha\mathbf{A}) - q_\alpha\nabla\phi, \tag{1}$$

$$\frac{d\mathbf{X}_\alpha}{dt} = \frac{1}{m_\alpha}(\mathbf{P}_\alpha - q_\alpha\mathbf{A}). \tag{2}$$

a)Author to whom correspondence should be addressed. Electronic mail: zwma@zju.edu.cn.

Electromagnetic fields **E** and **B** can be obtained from $\mathbf{E} = -\nabla\phi - \partial\mathbf{A}/\partial t$ and $\mathbf{B} = \nabla \times \mathbf{A}$ by solving the following Maxwell's equations:

$$\nabla^2\phi = -\alpha_e\rho, \tag{3}$$

$$\nabla^2\mathbf{A} = -\alpha_m\mathbf{J} + \frac{\alpha_m}{\alpha_e}\nabla\chi, \tag{4}$$

$$\nabla^2\chi = \alpha_e\nabla\cdot\mathbf{J}, \tag{5}$$

where $\chi = \partial\phi/\partial$t is the time derivative of ϕ, α_e, and α_m are electric and magnetic coupling constants. The initial conditions are given as a Harris sheet

$$n(z) = n_b + n_0\sec h^2(z/a), \tag{6}$$

$$B_x(z) = B_0\tanh(z/a), \tag{7}$$

where n_b and n_0 represent the particle number density of the uniform background and the center of the current sheet, respectively. When the temperature is uniform, B_0 is the asymptotic magnetic field in the upstream region, and a is the half-thickness of the current sheet. A detailed analysis of the relation between the peak reconnection rate E_r and a is given in Sec. III.

The field boundary conditions are open for both inflow and outflow boundaries, i.e., at the inflow boundary $z = \pm L_z$

$$A_x(x, \pm L_z, t) = A_x(x, \pm L_z, 0) = 0, \tag{8}$$

$$\partial^2 A_y(x, \pm L_z, t)/\partial z\partial t \pm V_A\partial^2 A_y(x, \pm L_z, t)/\partial z^2 = 0, \tag{9}$$

$$\partial A_z(x, \pm L_z, t)/\partial z = 0, \tag{10}$$

$$\chi(x, \pm L_z, t) = \chi(x, \pm L_z, 0) = 0, \tag{11}$$

$$\varphi(x, \pm L_z, t) = \varphi(x, \pm L_z, 0) = 0, \tag{12}$$

where V_A is the local Alfvén speed based on the boundary plasma density, and at the outflow boundaries $x = \pm L_x$

$$\partial A_x(\pm L_x, z, t)/\partial x = 0, \tag{13}$$

$$\partial^2 A_y(\pm L_x, z, t)/\partial x^2 = 0, \tag{14}$$

$$A_z(\pm L_x, z, t) = A_z(\pm L_x, z, 0) = 0, \tag{15}$$

$$\chi(\pm L_x, z, t) = \chi(\pm L_x, z, 0) = 0, \tag{16}$$

$$\varphi(\pm L_x, z, t) = \varphi(\pm L_x, z, 0) = 0. \tag{17}$$

Particle buffer zones are set up to handle particles moving across both inflow and outflow boundaries. Equation (9) is the magnetosonic (MS) boundary condition,[23] and other models were also used for open boundary simulations, such as zero-gradient (ZG) boundary $\partial^2 A_y/\partial z^2 = 0$ and electromagnetic (EM) boundary $\partial^2 A_y/\partial z\partial t \pm c\partial^2 A_y/\partial z^2 = 0$,[20] where c is the light speed. Some previous works show that for the open boundary cases with different inflow boundary conditions, the reconnection processes are nearly the same in the early stage when the reconnection rates have all reached their peaks. However, when the thickness of the initial current sheet is larger than the asymptotic ion gyroradius ρ_i, different boundary conditions have remarkable effect on the peak reconnection rate and even reconnection process in the early stage as shown in Sec. III.

The simulation runs on 512×256 grids, and the simulation lengths are $L_x = 2L_z = 25\rho_i$, where $\rho_i = V_{thi}/\Omega_{ci}$ is the ion gyroradius, $V_{thi} = (2T_i/m_i)^{1/2}$ is the ion thermal velocity, and $\Omega_{ci} = eB_{x0}/m_i$ is the ion gyrofrequency. The ratio of the background to the central current sheet particle density n_b/n_0 is 0.2. The mass ratio of ion to electron m_i/m_e is artificially taken as 25, and the temperature ratio T_i/T_e is set to 5. The plasma frequency-gyrofrequency ratio ω_{pe}/Ω_{ce} is taken to be 6, where the electron Langmuir frequency is defined by $\omega_{pe} = (n_0e^2/\varepsilon_0m_e)^{1/2}$. In our simulation, 1.0×10^8 particles for each species are loaded and the time step is $0.05\Omega_{ce}^{-1}$.

In this paper, we redefine the following variables to make them dimensionless: the time normalized by the inverse ion gyrofrequency Ω_{ci}^{-1}, the length by the ion gyroradius ρ_i, the electric field by $E_0 = B_0V_{A0}$, where V_{A0} is the ion Alfvén speed based on the density n_0 in the central current sheet, and the current density by $J_0 = B_0/\mu_0\rho_i$.

III. SIMULATION RESULTS

The reconnection process is triggered by the initial internal perturbation on the electric field, which is given as $E_r = e_0 \cdot \exp(-(x/x_0)^2 - (z/z_0)^2)/(\cosh^2((t-t_0)/t_1))$, with $x_0 = 1$, $z_0 = 1$, $t_0 = 2$, and $t_1 = 1$, while e_0 varies with the thickness of the current sheet in order to reduce the long duration of the linear growth phase. This type of the initial perturbation was employed before in the study of the MHD reconnection.[29,30] The peak reconnection rate is independent of the initial perturbation.

We conduct eight different initial half-thicknesses of the current sheet: $a = 0.3$, 0.4, 0.5, 0.7, 1.0, 2.0, 3.0, and 5.0. The reconnection rates as the function of time for different current sheet thicknesses are shown in Figure 1. We define the reconnection rate by the time derivative of the reconnected magnetic flux between the O and X points. It is evident that the peak value of the reconnection rate depends on the initial thickness of the current sheet. When the initial current sheet is thicker, the peak value of the reconnection rate is smaller, and it takes a longer time to reach it. For the cases with $a < 1.0$, reconnection processes have the similar trend in the

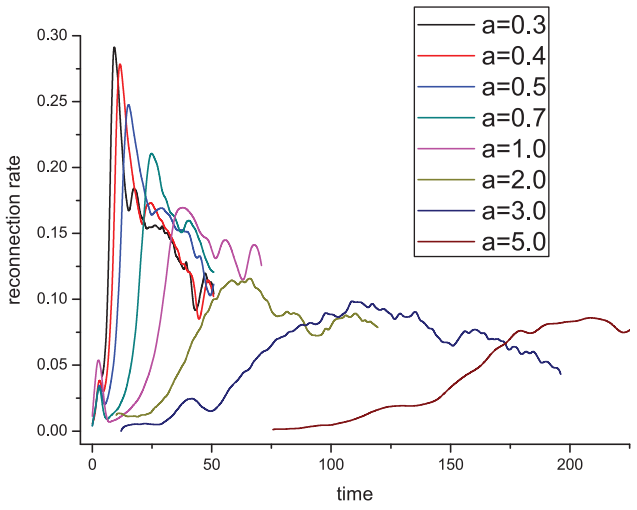

FIG. 1. The time evolutions of the reconnection rates with different initial current sheet half-thicknesses a.

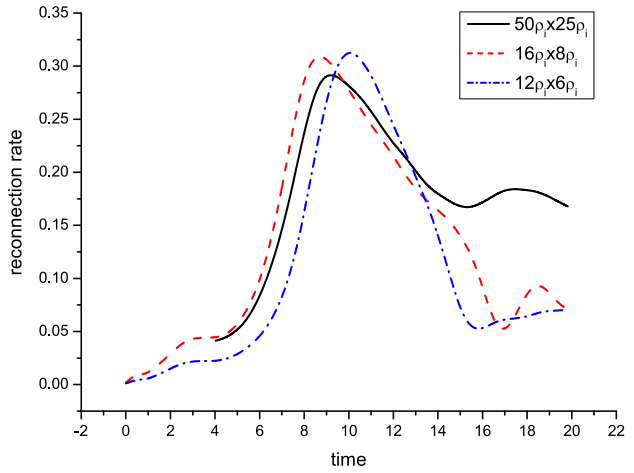

FIG. 2. All three runs have the same total mesh points, which means that the smallest system size $12\rho_i \times 6\rho_i$ has the highest resolution.

early stage. The reconnection process develops quickly after the initial perturbation. Once the reconnection rate reaches the peak value, it decreases immediately. The peak reconnection rates for $a = 0.3$, 0.4, 0.5, and 0.7 reach about $E_r = 0.293$, 0.278, 0.248, and 0.211 at $t = 9.1$, 11.6, 15.2, and 24.8, respectively. The reconnection for $a = 1.0$ decreases little slower than that for thinner current sheets after the reconnection reaches the fastest reconnection rate with $E_r = 0.169$ at $t = 37$. In the decaying phase, the reconnection process does not exhibit a monotonic decay and multiple enhanced reconnection processes are observed. With $a > 1.0$, the reconnection processes develop and decay much slowly. The peak rates are 0.114, 0.1, and 0.078 for $a = 2.0$, 3.0, and 5.0, respectively. It is notable that some following peaks may reach very high value, even higher than the first peak value due to the secondary tearing mode instability for some cases with the thicker initial current sheet. Hence, only the first peak value is meaningful for the scaling analysis of the reconnection rate and the initial current sheet thickness.

We conduct the convergent study for the small current sheet with $a = 0.3$. Figure 2 shows the reconnection rates with different resolutions. All three runs have the same total mesh points, which mean that the smallest system size $12\rho_i \times 6\rho_i$ has the highest resolution. The changes of the system sizes will not affect the peak reconnection rates for the case a = 0.3 because dynamic process of magnetic reconnection is still confined very locally around the X-point as shown in Figure 3. Figure 2 indicates that the peak

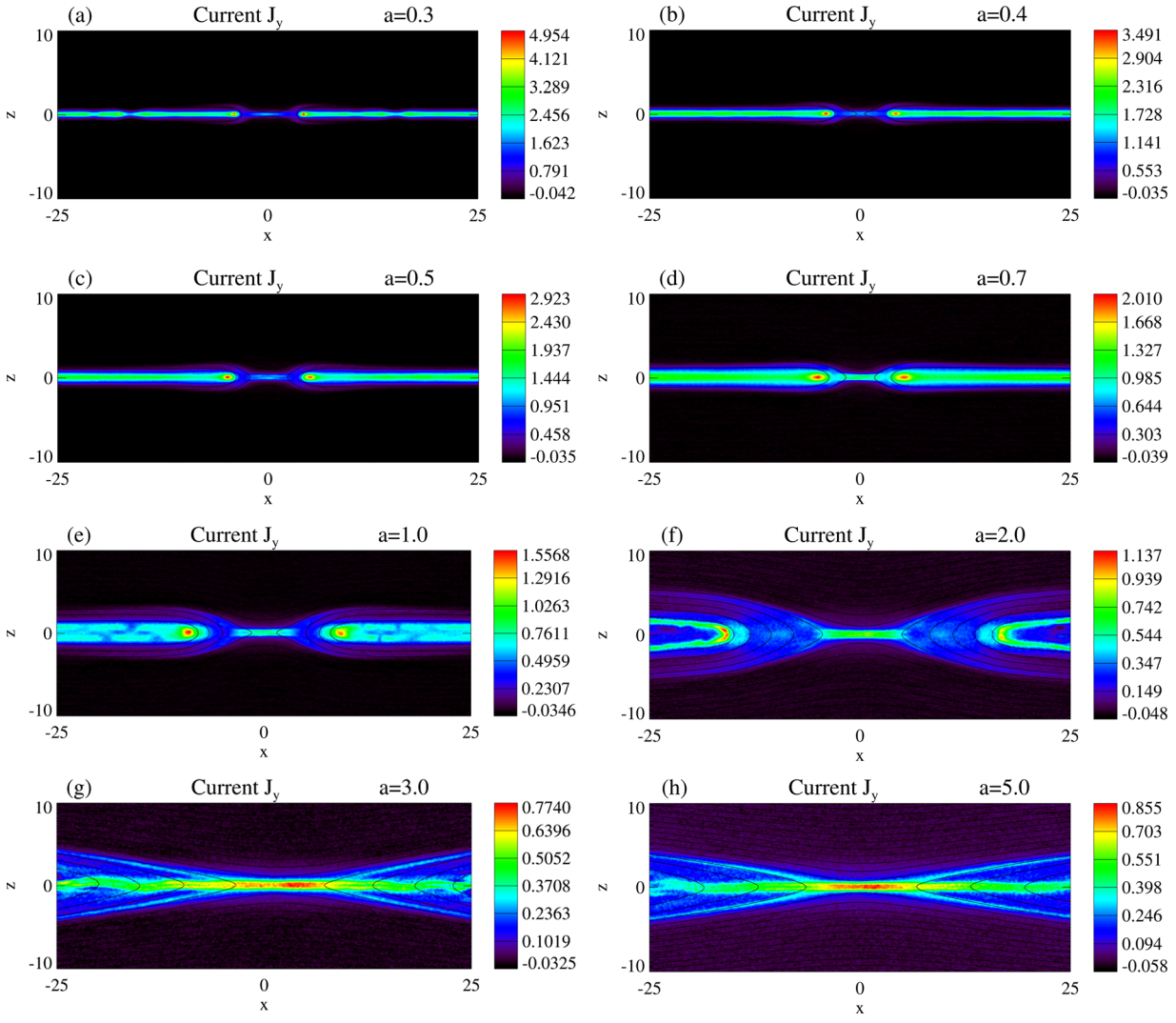

FIG. 3. 2D distributions of the current density Jy for different initial current sheet half-thicknesses when the reconnection rates reach their first peaks.

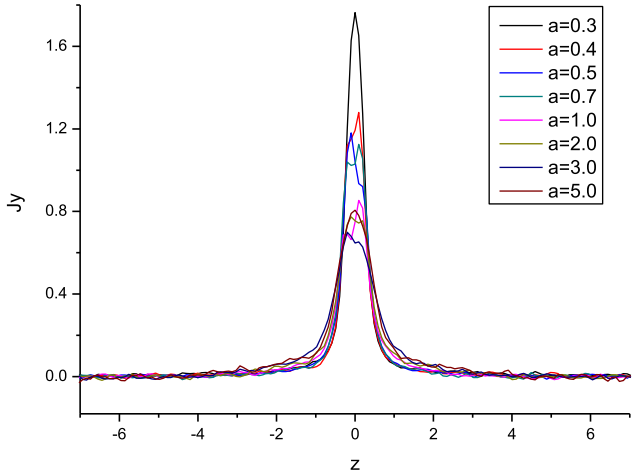

FIG. 4. Profiles of the current density J_y along the line $x = x_r$ for different initial current sheet half-thicknesses when the reconnection rates reach their first peaks.

reconnection rates remain nearly unchanged as the resolution increases. This result may suggest that the peak reconnection rate is insensitive to the local properties in the small reconnection region, which is consistent with that the reconnection rate in Hall MHD is nearly independent of the dissipation mechanism in the small reconnection region. But it should be noted that the reconnection rates in the late nonlinear phase, i.e., subsequent to the peak reconnection rate, are influenced by different numerical resolutions. This fact may be attributed to the under-resolution of the electron diffusion region in the PIC simulation. Micro-turbulence and wave-particle interaction should play an important role on the presence of a finite reconnection electric field in the reconnection diffusion region in collisionless plasma. The generation mechanism of the collisionless reconnection electric field in the diffusion region should be further studied by the PIC simulations with much higher numerical resolution around the X point.

Figure 3 shows the 2D distributions of the current density J_y superposed with the magnetic field lines for different half-thicknesses a when the reconnection rate reaches its first peak. It is found that the length of the reconnection current sheet increases with increase of the initial current sheet thickness; however, the thicknesses of the reconnection current sheet are nearly the same, which is shown more clearly in Figure 4. In Figure 4, the profiles of the current density J_y along the line $x = x_r$ with different initial current sheet half-thicknesses are plotted, where x_r is the X-point position in the x coordinate at the time with the first peak reconnection

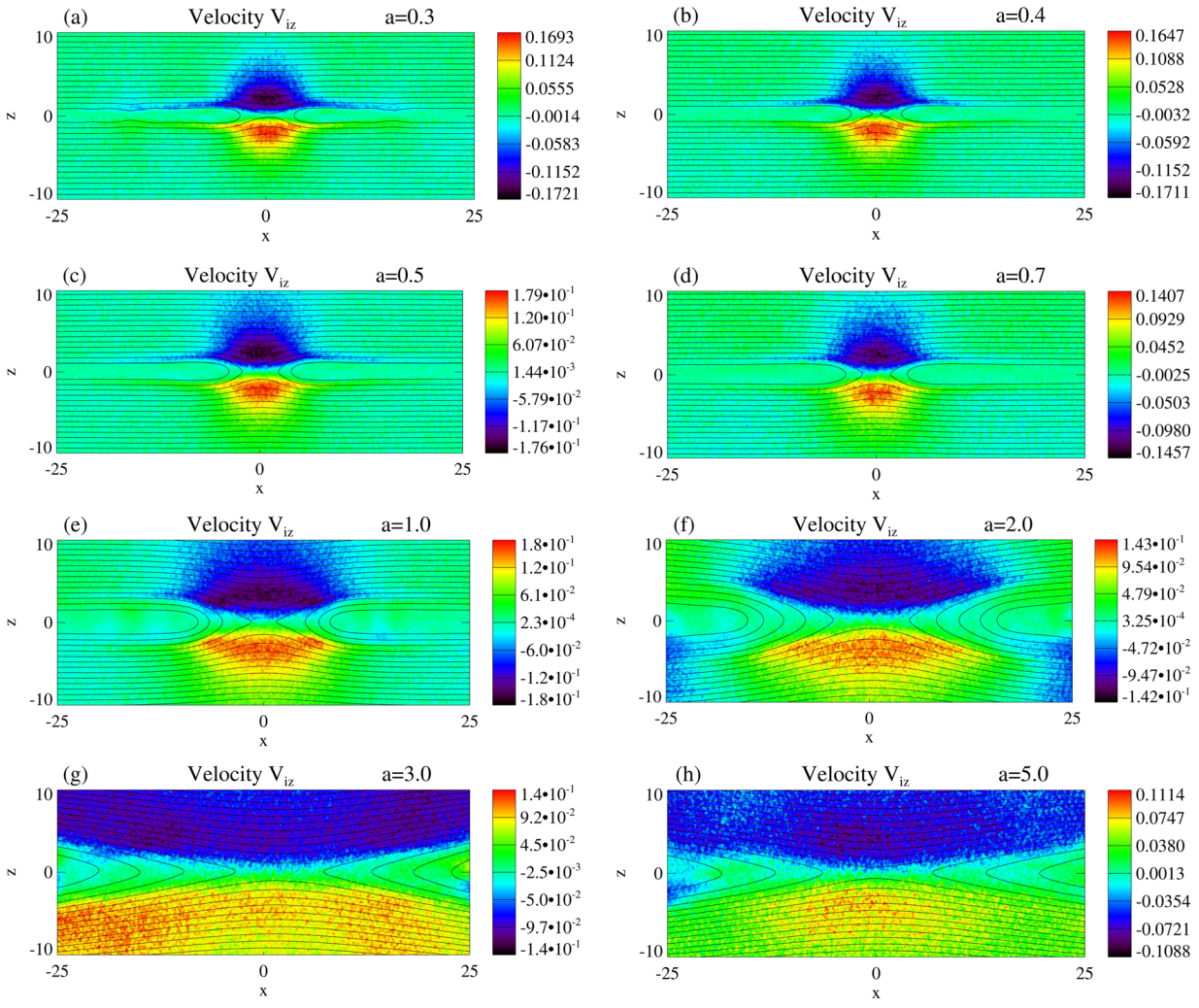

FIG. 5. 2D distributions of the ion flow velocity V_{iz} for different initial current sheet half-thicknesses when the reconnection rates reach their first peaks.

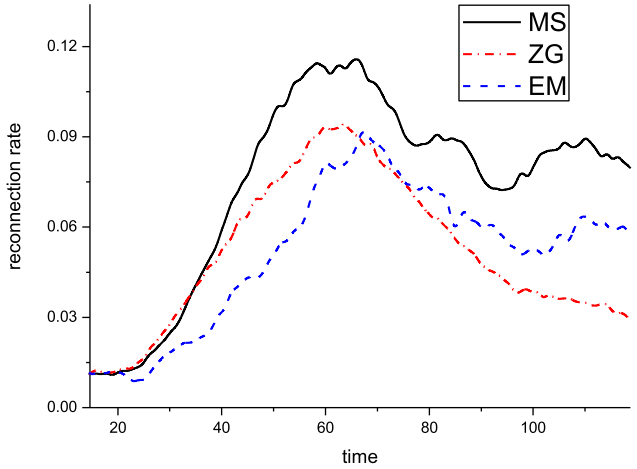

FIG. 6. The time evolution of the magnetic reconnection with the same initial current sheet half-thickness 2.0 and different inflow boundary conditions: MS boundary $\partial^2 A_y/\partial z\partial t \pm V_A\partial^2 A_y/\partial z^2 = 0$, ZG boundary $\partial^2 \mathrm{Ay}/\partial \mathrm{z}^2 = 0$, and EM boundary $\partial^2 \mathrm{Ay}/\partial \mathrm{z}\partial \mathrm{t} \pm \mathrm{c}\partial^2 \mathrm{Ay}/\partial \mathrm{z}^2 = 0$.

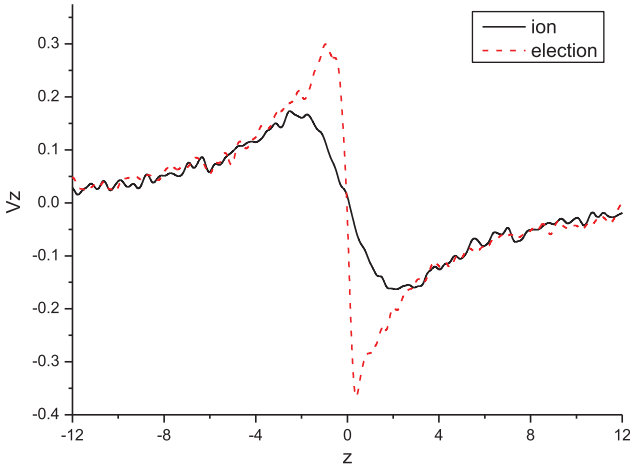

FIG. 8. Profiles of the ion inflow velocity V_{iz} and the electron inflow velocity V_{ez} along the line $x = x_r$.

rate. It is suggested that the thickness of the reconnection current sheet is almost the same, independent of the initial system size, and its value is about the ion gyroradius. On the other hand, the peak value of the reconnection current density decreases with the increase of the half-thickness a. From the above results, it can be speculated that the different peak reconnection rates must be associated with the different lengths of the reconnection diffusion region.

Figure 5 shows the 2D distributions of the ion flow velocity V_z superposed with the magnetic field lines for different current sheet thicknesses a at the time for the first peak reconnection rate. It is clear that when the initial current thickness is thicker, the ion inflow distributes a broader region. For the cases a = 3.0 and 5.0, the ion inflows almost reach the entire simulation domain, which explains why the length of the reconnection current sheet increases and the peak reconnection decreases with increase of the initial current thickness. When the half width of the initial current sheet is smaller than the ion gyroradius, the ion flow velocity at the inflow boundary is almost zero, and the region affected

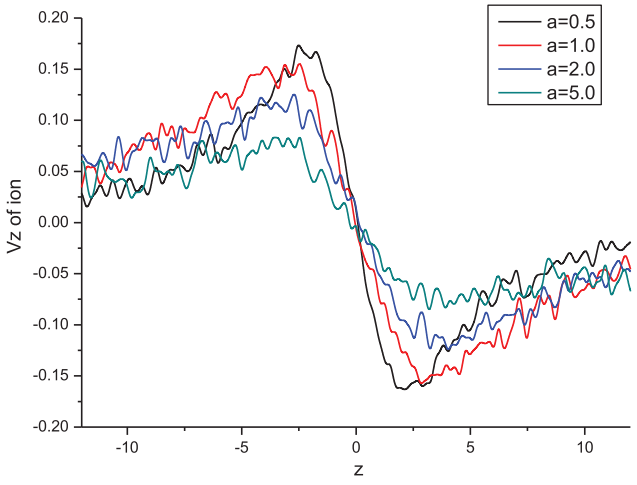

FIG. 7. Profiles of the ion inflow velocity V_{iz} along the line $x = x_r$ for different initial current sheet half-thicknesses.

by reconnection process is confined only in the surrounding area of the X-point and the peak reconnection rate will not be influenced by the inflow boundary. When the initial half width of the initial current sheet is larger than the ion gyroradius, there is the ion flow across the simulation boundary moving towards the reconnection diffusion region. At this time, the choice of boundary condition will directly influence the reconnection process. In Figure 6, three different boundary conditions, i.e., the MS boundary condition $\partial^2 A_y/\partial z\partial t \pm V_A\partial^2 A_y/\partial z^2 = 0$, the ZG boundary condition $\partial^2 A_y/\partial z^2 = 0$, and the EM boundary condition $\partial^2 A_y/\partial z\partial t \pm c\partial^2 A_y/\partial z^2 = 0$, are chosen for the cases with the initial half-thickness $a = 2$. It is evident that the case with MS boundary condition has a larger peak reconnection rate than the others. It may be suggested that the boundary condition may directly influence the scaling of the reconnection rate and the initial current sheet thickness.

Profiles of the ion inflow velocity V_{iz} along the line $x = x_r$ with different initial current sheet half-thickness $a = 0.5$, 1.0, 2.0, and 5.0 are illustrated in Figure 7. It can be seen that the peak speed of the ion inflow decreases with increase of the current sheet thickness. But the positions for the maximum inflow speeds remain almost unchanged, i.e., $z = \pm 2.5$, where electron and ion motions start to decouple each other, as shown in Figure 8. Figure 8 plots the electron and ion inflows at the peak reconnection rate for the case with initial half thickness $a = 0.5$, which leads to the fact that ion and electron motions decouple at $z = \pm 2.5$. The area in-between two decouple points is called ion diffusion region. From Figure 7, it is suggested that the width of the diffusion region is about 5 ρ_i, which is independent of the initial conditions.

The peak reconnection rate as a function of the initial current sheet half-thickness a is plotted in Figure 9. The numerical results of the first peak reconnection rate are represented by the square symbol and the analytic fitting line is given by the solid line. It is shown that the peak reconnection rate depends on the initial thickness of the current sheet, and the scaling between them satisfies $E_r \sim a^{-1/2}$ approximately, which agrees well with the previous analytical and simulation results from Hall MHD.[19]

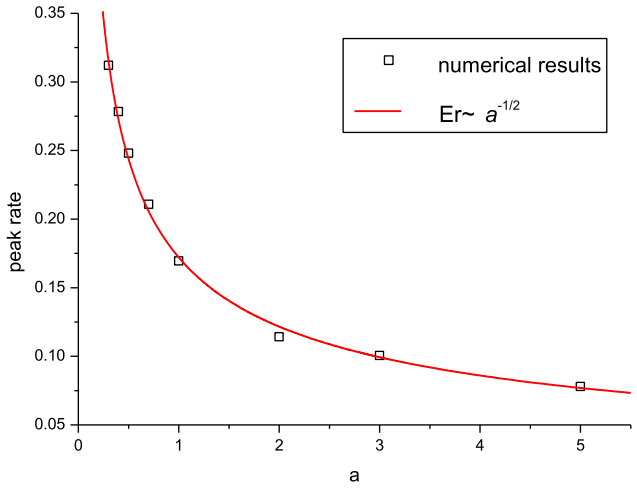

FIG. 9. The peak values of the reconnection rate as a function of the initial current sheet half-thickness a, demonstrating that it scales as $a^{-1/2}$.

IV. CONCLUSIONS

By using a $2\frac{1}{2}$-D Darwin PIC code, the dependence of the collisionless magnetic reconnection on the initial current sheet width is investigated. For the cases with different initial conditions, some reconnection properties such as the thicknesses of both the ion diffusion region and the reconnection current sheet are independent of the initial conditions while some other properties, e.g., the peak reconnection rates and the lengths of the current sheet, are dependent on it at the time that reconnection rate reaches its peak. This is due to the fact that the width of the ion diffusion region is fully determined by different responses of electron and ion motions to the magnetic field so that it is independent of the initial conditions of the magnetic field. While for spontaneous reconnection, the peak reconnection rate is closely determined by the releasing speed of the free energy of the system, which is determined by the initial conditions. The peak reconnection rate depends on the initial current sheet width with a scaling $E_r \sim a^{-1/2}$. For a very thin initial current sheet, the boundary does not affect the peak reconnection rate; while for thicker initial current sheet, the choice of the inflow condition has a large consequence on the peak reconnection rate. The MS boundary condition is applied to match these two parameter regimes. Another corollary of this work is MS boundary condition is a very good boundary condition for particle simulations in an open system.

It should be noted that the source of the reconnection electric field E_r or E_y is still poorly understood. From the electron momentum equation, we have

$$\mathbf{E} = \eta \mathbf{J} - \mathbf{v}_e \times \mathbf{B} - \frac{1}{ne}\nabla \cdot \vec{p}_e + \frac{m_e}{ne^2}\frac{D\mathbf{J}}{Dt}, \qquad (18)$$

where $\mathbf{v}_e$ and $\vec{p}_e$ are the electron velocity and the electron pressure tensor, respectively. In collisionless space plasmas, the classical resistive term and the electron inertial term in Eq. (18) become to be nearly zero for free electrons. In the low frequency regime, the $\mathbf{v}_e \times \mathbf{B}$ contribution can also be ignorable in the diffusion region. But, the reconnection electric field from the off-diagonal term of the electron pressure tensor may need to be considered because electrons are still weakly magnetized in the diffusion region as demonstrated in many PIC simulations, e.g., Ref. 31. In the MHD model, magnetic reconnection cannot occur because this off-diagonal term is always zero. In the high frequency regime, $\langle \delta \mathbf{v}_e \times \delta \mathbf{B} \rangle$, $\nabla \cdot \langle \delta \vec{p}_e \rangle$, and $\langle \delta \mathbf{v}_e \cdot \nabla \delta \mathbf{v}_e \rangle$ associated with plasma micro-turbulences and wave particle interactions can give rise to a reconnection electric field at the X-point. Hence, anomalous resistivities resulted from high frequency micro-turbulences and wave-particle interactions could be essential for MHD reconnection in space plasmas.[30]

ACKNOWLEDGMENTS

This work was supported by the National Natural Science Foundation of China under Grant Nos. 11175156 and 41074105, the China ITER Program under Grant Nos. 2013GB104004 and 2013GB111004.

[1]V. M. Vasyliunas, Rev. Geophys. **13**, 303, doi:10.1029/RG013i001p00303 (1975).
[2]D. Biskamp and E. Schwarz, Phys. Plasmas **8**, 4729 (2001).
[3]M. Mandt, R. Denton, and J. Drake, Geophys. Res. Lett. **21**, 73, doi:10.1029/93GL03382 (1994).
[4]D. Biskamp, E. Schwarz, and J. Drake, Phys. Plasmas **4**, 1002 (1997).
[5]M. Shay and J. Drake, Geophys. Res. Lett. **25**, 3759, doi:10.1029/1998GL900036 (1998).
[6]M. Shay, J. Drake, and B. Rogers, Geophys. Res. Lett. **26**, 2163, doi:10.1029/1999GL900481 (1999).
[7]B. Rogers, R. Denton, J. Drake, and M. Shay, Phys. Rev. Lett. **87**, 195004 (2001).
[8]M. Shay, J. Drake, and M. Swisdak, Phys. Plasmas **11**, 2199 (2004).
[9]J. Birn, J. F. Drake, M. A. Shay, B. N. Rogers, R. E. Denton, M. Hesse, M. Kuznetsova, Z. W. Ma, A. Bhattacharjee, A. Otto, and P. L. Pritchett, J. Geophys. Res. **106**, 3715, doi:10.1029/1999JA900449 (2001).
[10]M. Hesse, J. Birn, and M. Kuznetsova, J. Geophys. Res. **106**, 3721, doi:10.1029/1999JA001002 (2001).
[11]J. Birn and M. Hesse, J. Geophys. Res. **106**, 3737, doi:10.1029/1999JA001001 (2001).
[12]A. Otto, J. Geophys. Res. **106**, 3751, doi:10.1029/1999JA001005 (2001).
[13]M. A. Shay, J. F. Drake, B. N. Rogers, and R. E. Denton, J. Geophys. Res. **106**, 3759, doi:10.1029/1999JA001007 (2001).
[14]Z. W. Ma and A. Bhattacharjee, J. Geophys. Res. **106**, 3773, doi:10.1029/1999JA001004 (2001).
[15]P. Pritchett, J. Geophys. Res. **106**, 3783, doi:10.1029/1999JA001006 (2001).
[16]L. Yin, D. Winske, S. P. Gray, and J. Birn, J. Geophys. Res. **106**, 10761, doi:10.1029/2000JA000398 (2001).
[17]M. Ugai and T. Tsuda, J. Plasma Phys. **17**, 337 (1977).
[18]J. D. Huba and L. I. Rudakov, Phys. Rev. Lett. **93**, 175003 (2004).
[19]X. Wang, A. Bhattacharjee, and Z. W. Ma, Phys. Rev. Lett. **87**, 265003 (2001).
[20]R. Fitzpatrick, Phys. Plasmas **11**, 937 (2004).
[21]W. Daughton, J. Scudder, and H. Karimabadi, Phys. Plasmas **13**, 072101 (2006).
[22]K. Fujimoto, Phys. Plasmas **13**, 072904 (2006).
[23]J. Huang and Z. W. Ma, Chin. Phys. Lett. **25**, 1764 (2008).
[24]D. W. Swift, J. Geophys. Res. **91**, 219, doi:10.1029/JA091iA01p00219 (1986).
[25]D. Q. Ding, L. C. Lee, and D. W. Swift, J. Geophys. Res. **97**, 8453, doi:10.1029/92JA00304 (1992).
[26]H. J. Cai and L. C. Lee, Phys. Plasmas **2**(10), 3852 (1995).
[27]J. Huang, Z. W. Ma, and L. Ding, Geophys. Res. Lett. **35**, L10105, doi:10.1029/2008GL033751 (2008).
[28]Z. W. Ma, H. E. Sun, L. C. Lee, and A. T. Y. Lui, Phys. Plasmas **19**, 032904 (2012).
[29]M. Ugai, Plasma Phys. Controlled Fusion **26**, 1549 (1984).
[30]M. Ugai, Phys. Plasmas **19**, 072315 (2012).
[31]H. J. Cai and L. C. Lee, Phys. Plasmas **4**, 509 (1997).